14

Nanowires with Unimaginable Characteristics

Hui Li[1] and Fengwei Sun[2]
[1] *Key Laboratory for Liquid-Solid Structural Evolution and Processing of Materials, Ministry of Education, Shandong University, Jinan 250061,*
[2]*Physics Department, Ocean University of China, Qingdao, China*

1. Introduction

The understanding and functionalization of nanowires has become a topic of major interest to the international materials science and engineering communities due to their improved mechanical, electrical and thermodynamic properties. Molecularly perfect materials such as metallic nanowires have opened up opportunities for the design of nanometric electronic devices. Nanowires have a very large surface-area/volume ratio as compared to bulk materials, so their structures and properties can be quite different from those of bulk materials. Because of these unique properties, it is believed that nanowires will be utilized as the next-generation structural materials, biosensors, and as circuitry and interconnects in future nanoscale computers and micro-mechanical components.

This chapter presents the detailed analysis and explanation of how nanowires behave in the mechanical, electronical and thermal properties. In section 1, we focus on the mechanical properties and superplastic deformation of the 1-D carbon nanowires(CNWs). The objective of this work is to understand the tensile behavior of CNWs. And the key finding of this work is that the superplastic properties of CNWs and the stability of the elongated atomic chain emanating from CNWs may be due to the presence of a high strength multishell lattice structure that forms as an outcome of the plastically deforming nanowire(Li et al, 2008; Li et al, 2009). In section 2, we make some discussion on the electronical properties of metallic nanowires. A major issue in the use of them is the quality of electronic transmission, as obtaining the minimum resistance is critical to accessing their intrinsic electric properties. We use density function theory (DFT) to calculate Ni nanowires that are embedded in a carbon nanotube, and assess its applicability to the study of electronic transport along nanowires. These optimized stable structures of the ultrathin Ni nanowires in the carbon nanotubes are always multishell packs that are composed of coaxial cylindrical shells. The transmission of these nanostructures is dependent upon the geometric structures of nanowires and their size of diameters. Because of the quantum size effect, the current-voltage curves of the nanowires are clearly nonlinear, which does not follow an ohmic pattern(Li et al, 2007). In section 3, a microscopic description of the melting behavior of nanowire is simulated. We employed the well-fitted tight binding many body potential to investigate the heating process of the helical structure of Ni nanowires, which are obtained by the means of genetic algorithm (GA). Interestingly, we find that the melting of nanowire starts from the interior atoms which are different from bulk materials. When the slow heating rate is applied, the central atoms first move along the wire axis direction at a rather

Source: Nanowires Science and Technology, Book edited by: Nicoleta Lupu,
ISBN 978-953-7619-89-3, pp. 402, February 2010, INTECH, Croatia, downloaded from SCIYO.COM

low temperature, while the helical outer shells are almost invariant. It is worth noting that the moving central atoms are not discrete but to build up a long monostrand atomic chain. As the temperature arises, the regular monostrand atomic chain begins to become deformed and finally, the atomic chain is broken to form a new type of cluster(Li et al, 2005). The last section presents our conclusion.

2. Mechanical properties of nanowires and their composites

2.1 Simulation method

The numerical simulations are carried out by means of the classical molecular dynamics method (Ribarsky et al, 1988) in which Newtonian equations of motion are solved numerically for a set of atoms that interact via Brenner's ''second generation" empirical many-body bond order potential(REBO) (Brenner et al, 2002). Brenner's REBO potential energy has already been used to model the mechanical properties of carbon (Sinnott et al, 1988). But in the second-generation REBO potential, the switching function significantly influences the forces in the vicinity of the inflection point (Shenderova et al, 1999), so we modify the value of interaction cut-off. Huhtala et al. (Huhtala et al, 2004) used another simulation method that is adaptive intermolecular reactive empirical bond order (AIREBO) potential (Stuart et al, 2000) to study the mechanical load transfer between shells of multiwalled carbon nanotubes. Sammalkorpi et al. (Sammalkorpi et al, 2004) used the reactive analytical bond order potential model parametrized by Brenner but modified the cut-off value to avoid the overestimation of the force required to break a bond (Belytschko et al, 2002). These three methods are all indispensable extensions to the well-known reactive empirical bond order Brenner potential. The superplastic behavior of CNWs is simulated by solving the equations of motion using Gear's predictor–corrector algorithm (Gear, 1971). The axial tension of perfectly structured CNWs with different diameters and lengths is achieved by applying a rate of 10 and 80 m/s for CNWs, respectively. The end atoms are then moved outward along the axis by small steps and followed by a conjugate gradient minimization method while keeping the end atoms fixed (Liew et al, 2004). The simulation is carried out at approximately 1 K to avoid thermal effect. Similar research on the carbon tube has been done by Wang et al. (Wang et al, 2007) at the same temperature. Each time step used in this simulation is 1 fs, and the simulations are allowed to run for 500,000 time steps. Although many researchers have carried MD simulations of nanowires using schemes such as Nose-Hoover thermostat (Nose, 1984; Hoover, 1985), we note that under high rate at the time scale of the dynamic deformation of CNW, there is usually no effective mechanism for heat to be conducted. So we provide a more realistic condition of the dynamic deformation of CNWs, using no temperature controlling algorithms. CNWs are obtained by means of the Materials Studio(MS) software package. We adopted a molecular dynamics-based "simulated annealing"(SA) method to perform structural optimization to obtain the nanowire which is used to be stretched.

2.2 Results and discussion

2.2.1 Superplasticity of carbon nanowires

Figure 1 shows two snapshots of the CNWs at the initial state. The lengths of CNWs A1 and A2 are 47.4 Å and 50.5 Å, respectively. The CNWs are all multishell packs with each shell formed by rows of atoms that are helically wound upward side by side. CNW A1 features four-strand packing, and CNW A2 is composed of six-strand atomic rows.

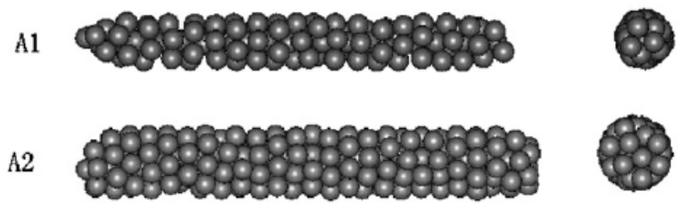

Fig. 1. Morphologies of carbon nanowires

CNW A1 undergoes superplastic deformation during the simulation process. The surprising result is that the maximum tensile strain, increases to nearly 245% before tensile failure. This superplastic deformation is the result of the slippage of carbon atoms as well as the intense interaction between them. Figure 2 shows the morphological changes of CNW A1 at different strains. The CNW becomes thinner and even in the middle to form a single atomic chain at ε=0.246. Further tension leads another part to become a single chain, as shown in Fig. 2(a) at ε=0.95. Eventually, the middle part becomes a single chain. When it is stretched completely, the initial CNW becomes an individual atomic chain with a diameter of one carbon atom. The whole process can be displayed by movie and is found to be very similar to drawing a thread from a silk cocoon. After it breaks, the carbon atomic chain is found to recoil and displays elastic-plastic behavior, as shown in Fig. 2(f).

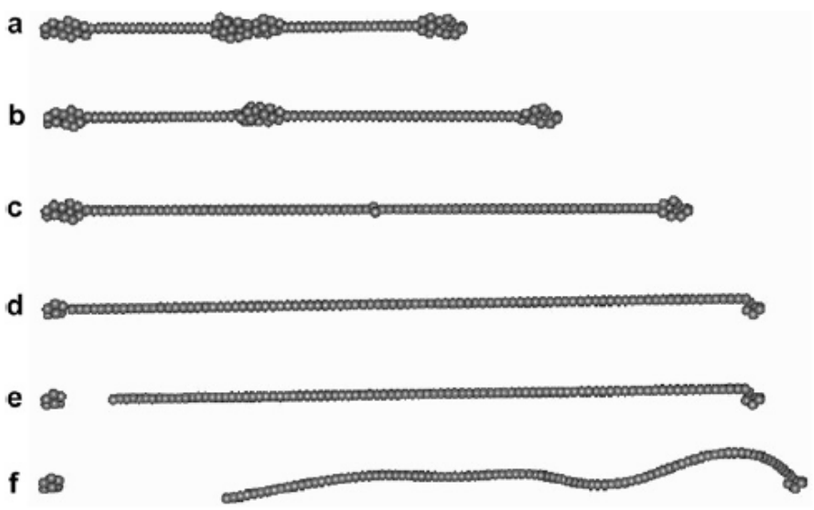

Fig. 2. There-dimensional views of morphological changes (axial deformation) for CNW (A1). (a) At ε=0.95 the two parts become a single chain. (b) At ε=1.42. (c) At ε=2.09 the middle part stretches to form a single chain and the stress is the largest (16.65Gpa). (d) At ε=2.45 the CNW is fully stretched. (e) At ε=2.457 the chain breaks. (f) After it breaks, the chain recoils.

In Fig. 3(a), the black curve indicates stress–strain relationship of the CNW A1. During the tensile straining, the stress–strain curve fluctuates corresponding to the fluctuation of the total potential–strain curve. This fluctuation mainly results from the slippage of carbon atoms from their spots. As one atom slips from one spot to another, the stress and the total potential spontaneously change from the peak value point to the valley point. Figure 3(a)

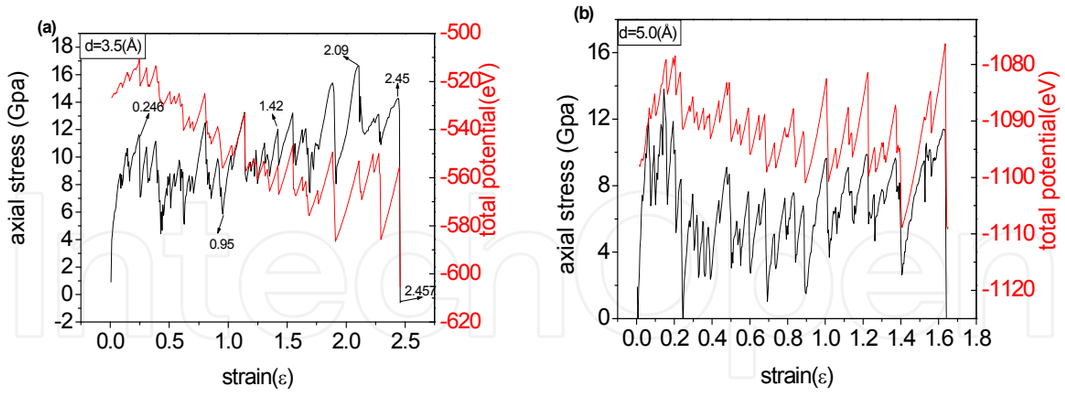

Fig. 3. (color online) Stress-strain and total potential-strain curves for CNWs with different diameters. (a)d=3.5Å(A1), (b)d=5.0Å(A2). The black curves correspond to stress-strain relationship, while the red curves correspond to total potential-strain relationship.

shows that the maximum stress for a CNW is 16.65 GPa. The red curves in Fig. 3 show the potential-strain relationship for CNWs with different diameters. When the strain increases, (as shown in Fig. 3b), the potential increases stair-like during the stretching process. But there is a little different trend for CNW with a smaller diameter in Fig. 3(a). Although the potential of the structure decreases with increasing the strain, it reflects the structure variation from complex sp3 hybridization to sp hybridization. At the initial stage, the structure (A1) was minimized to obtain the stable structure model. Some carbon atoms located in the center axis are surrounded by circumambient atoms. So the central carbon atoms will suffer strong interaction. During the stretching process, the single atom chain first forms from where C–C bond energy is weaker. The bond angle between carbon atoms at the joint is stretched to the degree of 180° to form the sp hybridization. As the stretching process continues, the number of carbon atoms surrounding the single atomic chain within the cut-off value becomes less, so the interaction between them becomes weak, in addition, sp hybridization is weaker than the sp3 hybridization. In order to explain clearly, we present the graphs which show the number of C atoms with different coordination numbers in Fig. 4.

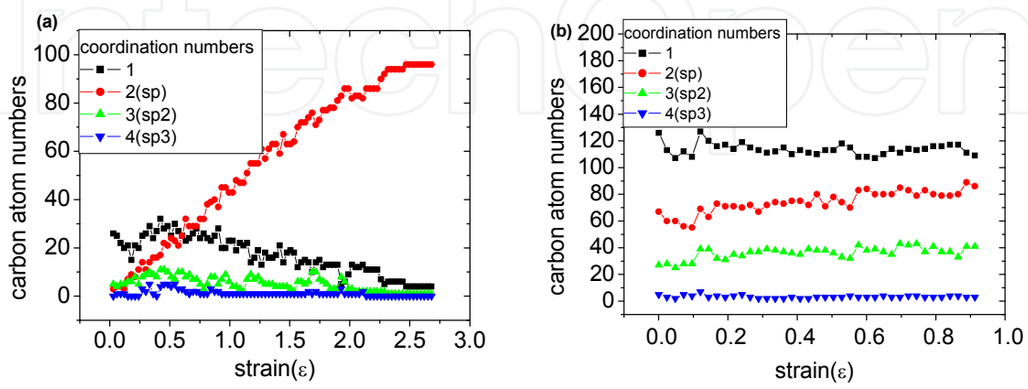

Fig. 4. (color online) The relationship between the number of C atoms with different coordination numbers (1,2,3,4) and the strain.(a) CNW with d=3.5 Å (A1) (b) d=8.5 Å.

As to the superplastic CNW A1, the number of C atoms forming sp hybridization increases as the stretching continues. And the number of sp2 and sp3 bonded atoms does not significantly increase during the pulling. The energy needed for CNWs (A1 and A2) to break are 8.17×10^{-10} nJ and 7.69×10^{-10} nJ, respectively, which are a little larger than the energy required to break a single C–C bond (5.76×10^{-10} nJ). As to CNWs with larger diameters, the number of C atoms forming sp hybridization does not vary remarkably as shown in Fig. 4b.

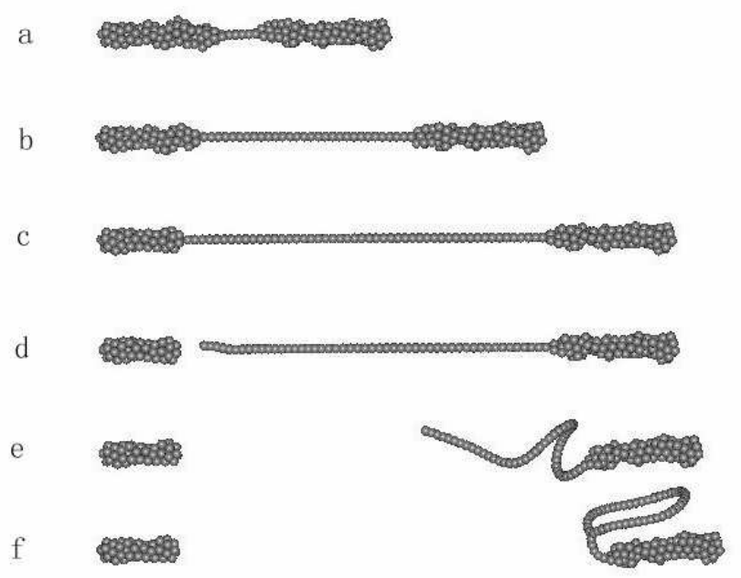

Fig. 5. Three-dimensional views of morphological changes (axial deformation) for CNW (A2) (a) At ε=0.25 the middle part forms a single chain. (b) At ε=1.0 the atomic chain stretches further. (c) At ε=1.62 the CNW has stretched to the maximum. (d) At ε=1.63 the atomic chain breaks. (e) The broken end recoils. (f) The broken end recoils, meeting with the single chain to form a loop.

Figure 5 shows CNW A2 at different strains. This is similar to the tensile process of CNW A1, but when CNW A2 breaks at ε=1.63 it appears to have not only superplasticity, but also elasticity. Figure 5 (e) and (f) clearly show that the broken end recoils and touches the single string to form a covalent bond loop. Figure 6 illustrates the maximum tensile strain of CNW as a function of the diameter of CNW. As the diameter increases from 3.5Å to 12.1Å, the maximum tensile strain decreases by nearly two thirds, i.e. from 245% to 82.3%, so the superplastic characteristics disappears while the diameter of CNW is larger than approximate 8Å. In contrast to CNW, maximum tensile strain of single walled carbon nanotube (SWCNT) with the diameter ranging from 6.26 to 13.56 Å is approximately 25~35%. Although the strength of SWCNT (Asaka et al, 2005; Ogata et al, 2003), multi-walled nanotubes (MWNTs) (Liew et al, 2004) and SWCNT bundle (Yu et al, 2000) are higher than CNW, but their maximum tensile strain are about 30%, 28%, 5.3%, respectively, much less than CNW.

2.2.2 Formation of nanobridge

In this section, we present an extensive set of simulation results for CNW encapsulated into carbon nanotube(CNT) to elucidate the mechanical properties of this material. Figure 7(a)

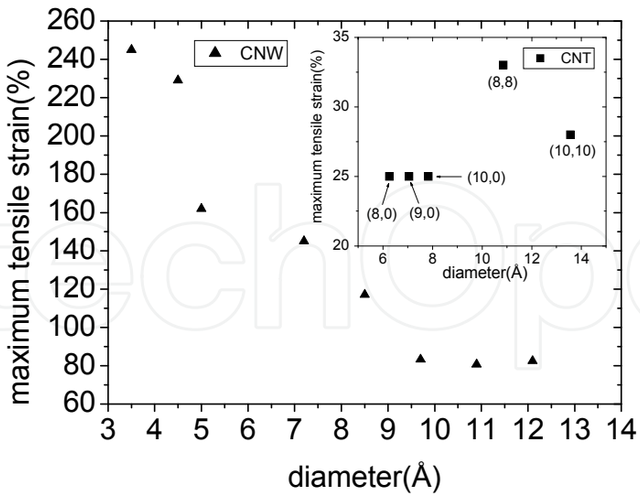

Fig. 6. The relation between maximum tensile strain and diameter of CNW. For comparison, the maximum tensile strains for SWCNT with different diameters are inserted.

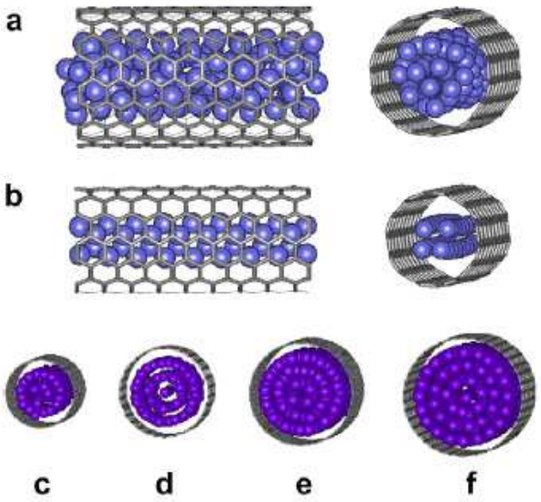

Fig. 7. (color online) Morphology of different CNTs encapsulating CNW.
(a)CNW@CNT(9,9). (b) CNW@CNT(7,7). (c) CNW@CNT (20,0). (d) CNW@CNT (15,15). (e) CNW@CNT (30,0). (f) CNW@CNT (20,20).

shows the morphology of an 11-strand CNW@CNT(9,9) (i.e., an 11-strand nanowire including 102 atoms with a helical structure that is encapsulated in a CNT(9,9)). Its length and diameter are 21.9 Å and 12.22 Å, respectively. The atoms that constitute the CNW are colored blue for clarity.

In the initial stage, the average distance between the outer atoms of the CNW and the CNT wall is about 3.16 Å, so the interaction between them is the long-rang van der Waals potential using the Lennard-Jones potential (Lennard-Jones, 1924). The stretching process of an 11-strand CNW@CNT(9,9) is shown in Fig. 8.

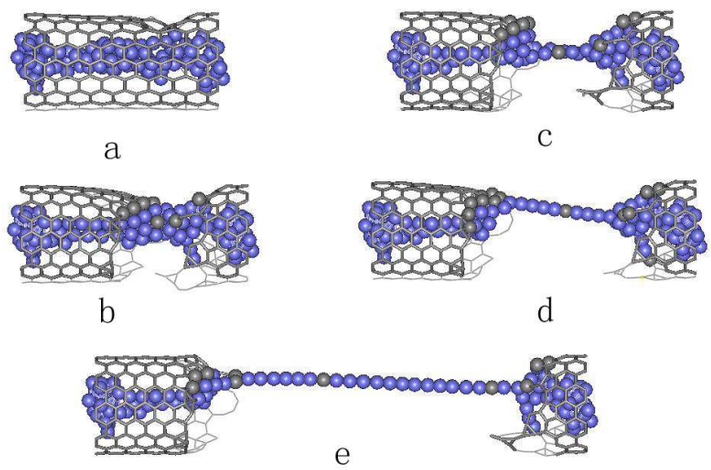

Fig. 8. (color online) Morphological changes of the 11-strand CNW@CNT(9,9) under elongation.(a) ε=0.22, the CNT begins to break and the CNW atoms attach to the surface of the CNT wall.(b) ε=0.51, the CNT fractures completely, and the CNT atoms and CNW atoms combine. (c) ε=0.91, the CNW begins to deform into a single chain. (d) ε=1.36, the single chain is stretched and the gray atom is composed of the initial CNT. (e) At ε=2.8, the CNW@CNT reaches its critical dimension.

There is a uniform increase in the C-C bond length, and the CNT atoms remain in their hexagonal structure. No defects are detected below the strain ε=0.22. As the strain reaches ε=0.228, the diameter of the tube apparently reduces and the necking effect (Troiani et al., 2003) is observed, as shown in Fig. 8(a). This is mainly because pentagon-heptagon dislocation (5|7) defect (Nardelli et al, 1998) dispersion occurs during the stretching process.

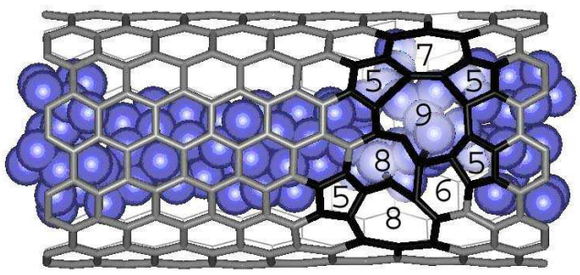

Fig. 9. (color online) Snapshot of the molecular dynamic simulation of the 11-strand CNW@CNT(9,9) at ε=0.228. The nucleation of the pentagon-heptagon dislocation can be seen, and much larger open rings form.

To show clearly the result, we present an atomic view of defect nucleation for CNW@CNT(9,9) in Fig. 9. As diameter of the CNT decreases, the interaction between the outer atoms of the CNW and those at the tube becomes stronger. And it results in forming a more complex hybridization structure; C-C bond can be rotated and some parts of the initial perfect hexagons are activated to form 5|7 defect during the elongation, then defect disperses all over the tube wall. With the combined effect of tension and rotation of C-C bond, some higher order rings such as octagon and nonagon are observed. The tube tension releases its excess strain via the spontaneous formation of topological defects. The closest

distance between the atom of the CNW and one of the CNT is 1.41 Å at ε=0.38 (in general, sp3 hybridization occurs at the distance of 1.54 Å). Recent density functional-theory simulation (Lehtinen et al, 2003) indicated that carbon atoms would form covalent bonds with graphene sheets thus affecting shell sliding. Experiments (Strano et al., 2003) also provided evidence that C–C covalent bonds can exists on the surface of a perfect nanotube. As the strain continues to increase, the cylinder of the CNT breaks (as shown in Fig. 8b). Finally, the composite structure is found to be a single carbon atomic chain between the CNT's fragments. The bonds in the linear chain are found to be of a cumulene type (i.e., all of the bond lengths are nearly equivalent), as shown in Fig. 8 d and Fig. 8 e. The potential energy undergoes a critical point to override the energy barrier. When the CNW@CNT starts to form single chain, the potential energy curve reveals fluctuation. Furthermore, this nanobridge structure resembles the experimental result of pulling out a long carbon nanowire at the end of a carbon nanotube (Rinzler et al, 2003). And in theoretical aspect, Wang et al. has also used the same MD simulation method to obtain a long stable single carbon nanowire by pulling some corner atoms of a graphite layer (Wang et al, 2007). Both of them obtained the stable single chain structure employing different methods.

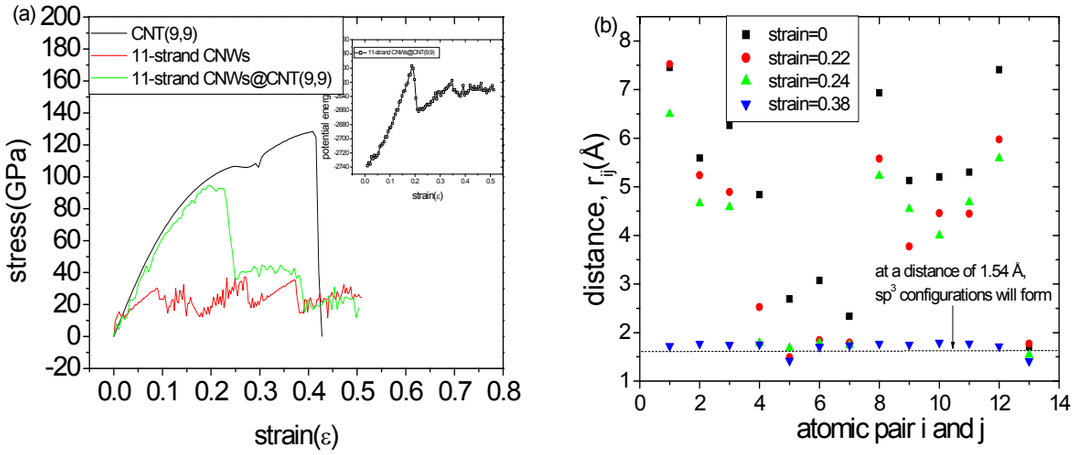

Fig. 10. (color online) (a) Stress-strain curves for the CNT(9,9), 11-strand CNW, and 11-strand CNW@CNT(9,9). Potential energy versus strain for the MD simulation of the stretching of the 11-strand CNW@CNT(9,9) is inserted. (b) Distances between selected atoms from the CNW and CNT at different strains.

Figure 10(a) shows the stress-strain curves for the individual CNT, CNW, and CNW@CNT at the same stretching rate. The critical stress for the CNTs is 127 Gpa, which is in good agreement with the experiment value (150Gpa) obtained by Demczyk (Demczyk et al, 2002). The critical stress of the CNW and CNW@CNT are 35Gpa and 94Gpa, respectively. The strength of the CNT is much larger than the composite nanostructure made up of CNW inserted into CNT. Insertion of the CNW into CNT does not increase the critical strength of the CNT, but actually weakens it. This is mainly because during the stretching process, the atoms of the CNW attach to the defect of the CNT, causing the bond to bend. As the strain increases, the 5|7 defect becomes a large "hole" that accelerates the fracturing of the CNT. The figure of how the potential energy for CNW@CNT(9,9) varies during the elongation is also inserted in Fig. 10(a). It rises steadily until a few C-C bonds break and simultaneously

rearrange themselves to form a 5|7 defect. As the defect becomes larger, the potential energy decreases. At the same time, the atoms of CNW attach to the breaking fragment of the CNT to form a new strong covalent bond. As the strain increases, the fracture quickly propagates along the surface of the composite structure. The latter fluctuation of the curve is mainly the result of the gliding of the carbon atoms. As an atom slips from one spot to another, the total potential changes spontaneously from a peak to a valley. Figure 10(b) depicts the distance between a selected pair of atoms, one of which is from the CNT and the other is from the CNW. At ε=0.22, the potential reaches the maximum, and the distances of the four pairs of atoms reaches about 1.54 Å. Between ε=0.22 and ε=0.24, the CNT begins to break away from the circumference of the tube, and the potential energy falls steeply. At ε= 0.38, the distance between the 13 pairs of atoms approaches 1.54 Å, which lead to a complex hybridization that causes an increase in the potential energy.

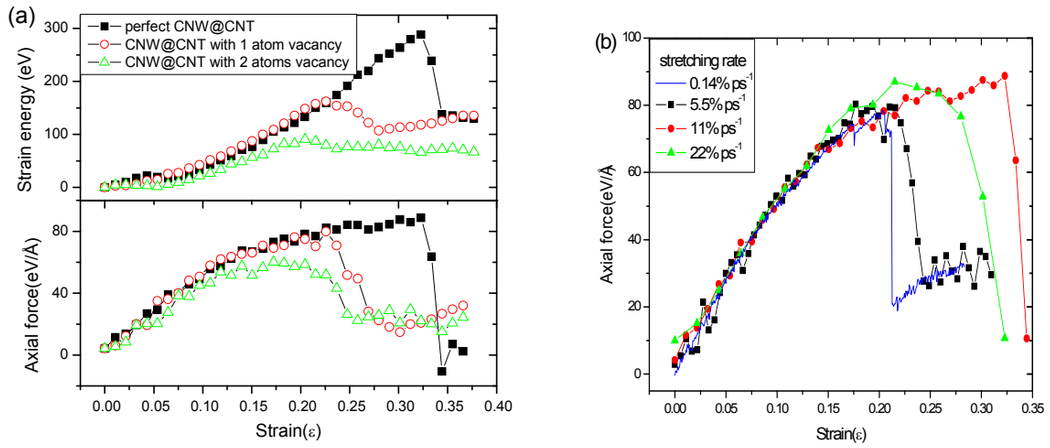

Fig. 11. (color online) (a) the upper one shows the relationship between strain energy and strain for perfect CNW@CNT and CNW@CNT with vacancy. The lower one shows the axial force as a function of strain for CNW@CNT as referred. (b) Axial forces as a function of strain under different stretching rates.

CNT exhibits mainly brittle behavior at high speeds, whereas the CNW@CNT shows apparent flexibility and plasticity. In contrast to our research, Marques et al. predicted that under high temperatures and in the presence of defects (Stone-Wales or vacancies) the tube would exhibit mainly plastic deformation, and the stretching tube would form a single wire composed of fourteen atoms. He (Marques et al, 2004) suggested that such defects (Stone-Wales or vacancies) play an important role in the plastic dynamics of the necking and thinning of a CNT. In order to show how the vacancy defect of CNT affects the stretching behavior of CNW@CNT, we present the variety of strain energy and axial force in the tensile process in Fig. 11(a). The solid square curve corresponds to CNW embedded into perfect CNT(9,9). The hollow circle and triangle curves correspond to CNW embedded into CNT with one atom and two atoms vacancy, respectively. From the upper one in Fig. 11(a) showing the strain energy as a function of strain, CNW embedded into perfect CNT needs higher energy to override the barrier than the other two types. Furthermore, the strain energy curve suffers a sharp drop after the critical point. As the atom vacancy increases, the energy barrier decreases and the curves vary smoothly after the critical point. The lower one

in Fig. 11(a) also shows the CNW embedded into perfect CNT can suffer higher axial force than the other two types. Figure 11(b) shows the computed force-strain relationship of the CNW@CNT under different stretching rate ranging from 5.5%ps^{-1} to 22%ps^{-1}. The curves show nonlinear effects before the critical point. The critical forces are 79.2, 88.7 and 87.0 eV/Å under the rates 5.5%ps^{-1}, 11% ps^{-1} and 22% ps^{-1}, respectively. Furthermore, the critical strain does not decrease as the stretching rate increases. The critical strain under stretching rate 5.5% ps^{-1} and 11% ps^{-1} are 22.5%, 32.3%, respectively. This is mainly due to the thermal fluctuation effect under lower stretching rate. This interesting result is similar to the experimental result of stretching nanocrystalline copper (Lu et al, 2001). As the stretching rate increases, some C-C bonds between atoms stretch larger in a shorter time. This abrupt variety in the structure leads to fracture easily. There is usually a modest stretching rate under which the critical strain of this kind of nano scale materials reaches the maximum.

3. Electronic properties of nanowires

The researches on the electron transport through small metallic and semi-conductor nanowires have been a topic of interest over the past few decades. There has also been tremendous interest in the use of metallic nanowires as molecular electronic devices(Krans et al, 2002). Many theoretical studies of ultrathin nanowires or some straight-line uniform ultrathin nanowires with helical multishell structures have been conducted using the atomistic simulation of several metals, and shows other simple and transition metals have found no better linearity for nanowires than that displayed by gold (Sen et al, 2001). Single atomic chains have been prepared by molecular-beam epitaxy on ordered stepped surfaces that are distinguished by an inherent periodic one-dimensional pattern. This widely applicable technique permits the preparation of large-area nanostructures of outstanding quality. Another method that has been used to produce very thin wires and study their structure is the electron beam irradiation of a Au(100)-oriented thin film(Kondo et al, 2000). Several approaches have been used to study the conductance of metallic nanowires, showing conductance curves with plateaus and jumps, but displaying different profiles (Rodrigues et al, 2000). Garcia and Burk(Garcia et al, 1997; Burki et al, 1999) calculated the conductance of disordered nanocontacts and showed that electron scattering due to random impurities shifts nG_0 peaks to lower values and reduces their heights. A strong impurity scattering was predicted by Brandbyge et al., who showed that an electron scatter located at the center of a nanocontact almost washes out the $1G_0$ conductance peak (Brndbyge et al, 1997). Sakai(Enomoto et al, 2002) measured the quantized conductance of Au-Pd and Au-Ag alloy nanocontacts for a wide range of Pd and Ag concentrations and studied how the $1G_0$ conductance of Au changes with alloying. Despite all this progress, only few studies have been conducted on the atomic structures of metallic nanowires and their electrical transport properties. Thus, the objective of this chapter is to use atomistic simulations to systematically study the structures of Ni nanowires and explain the correlation between the electron conductance and atomic structures.

3.1 Simulation method

All the calculations were performed using MS molecular modeling software packages. These nanowires are firstly optimized by molecular dynamics (MD) based method such as the module of DISCOVER, Forcite or SA method to perform structural optimization. Then

the low-energy configurations from the above MD simulation within the empirical potential were further optimized using density function theory (DFT) with the Perdew-Burke-Ernzerh exchange correlation function (Perdew et al, 1996) and an all-electron basis set of the double-numerical-plus-d-polarization type, as implemented in the DMOL package. In the DFT optimizations, both the atomic coordinates and 1-D super cell lengths along the wire axis were fully relaxed.

The current-voltage *(I-V)* characteristic and electron transmission probability were calculated using the nonequilibrium Green function (NEGF) formalism and density functional theory (DFT) which determined the *I-V* characteristics and transmission of nanowires sandwiched between the two metallic contacts, one of which could be a scanning probe. NEGF provides a powerful conceptual and computational framework for treating quantum transport in atomic-level materials, such as nanotubes, nanowires, and moleculars. The calculation details are given as follows:

The primary objective of this stage is to specify the structure of the nanowire. The nanowires and their geometry connected with gold atoms of the contact to form covalent bond. The nanowire-contact distance that we used is constant when different nanowires were connected to contacts. Gold (111) films were used as electrodes and the nanowires were perpendicularly sandwiched between the electrodes. The vertical distance between the end atoms of the nanowire and the gold contacts was set to 1.900 Å. The self-consistent-field approach is coupled with nonequilibrium Green's function (NEGF) formalism to describe electronic transport under an applied bias (Damle et al, 2002). The whole system is divided into a contact subspace and a nanowire subspace. This makes the simulation procedure simple to implement.

3.2 Electrical transport properties of Nickel nanowires

The optimized structures of Ni nanowires are shown in Fig. 13, where the number of inserted Ni atoms is 8, 16, 16, 24, and 30. In our simulations, an 8-atom stable single chain was obtained as Wire 1. Wire 2 formed in CNT(9,0) is an optimized double-chain structure that is composed of two parallel single chains in which the atoms are arranged in an interleaving fashion. Wire 3, another stable nanowire formed in CNT (9,0) is made up of two helical strand of atomic chains. Wire 4 features three-strand packing, and Wire 5 is a nonhelical shell structure. In general, the stable structures of the ultrathin Ni nanowires in the carbon nanotubes are multishell packs that are composed of coaxial cylindrical shells. In some cases, the nickel nanowires have a single-atom chain at the center. Each shell is formed by rows of atoms that are helically wound upwards side by side.

The transmission probability *(TE)* is dependent on the microstructure as shown in Fig. 14(a), for the *TE* of wire 2 with two parallel atomic chains is larger than Wire 3 with a helical structure. Transmission properties of the systems are determined by the electronic structure of the combined nanowire and electrode systems. The distance between the electrodes plays an important role in the current of the junction. In simple terms, the metal-nanowire-metal system can be viewed as a finite quantum well that sets up in between the metal surfaces. The direct tunneling between the electrodes, despite the possible electrode-induced gap states in the metal-air-metal junctions, is considered to be too small to contribute considerably to the current of the typical size molecular junctions. Interestingly, shown in Fig. 14(c), the shape of the curve of the single chain (wire 1) is markedly different from that of the chain that is embedded in the carbon nanotube. Ke and Baranger(Ke et al, 2006) investigated electrical transport in the nanotube-metal junctions of carbon tubes surrounded

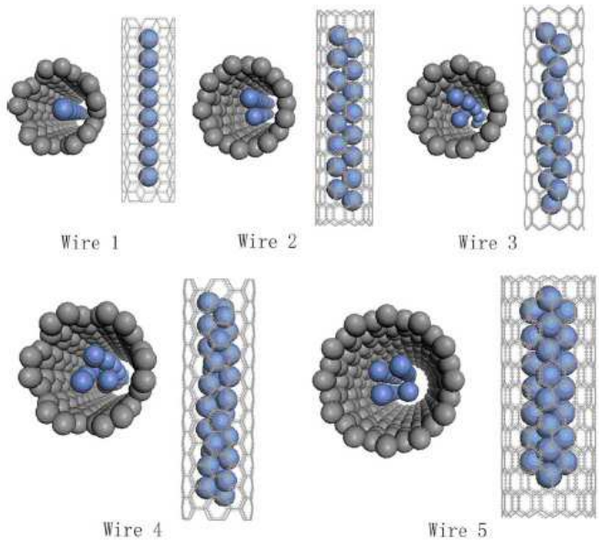

Fig. 13. (Color online) Images of the metallic nanowires with different diameters: Wire 1, single atomic chain; wire 2, double chain composed of two parallel atomic chains; wire 3, helical double atomic chain; wire 4, helical shell structure wound by three atomic strands; wire 5, shell structure composed of four parallel atomic chains.

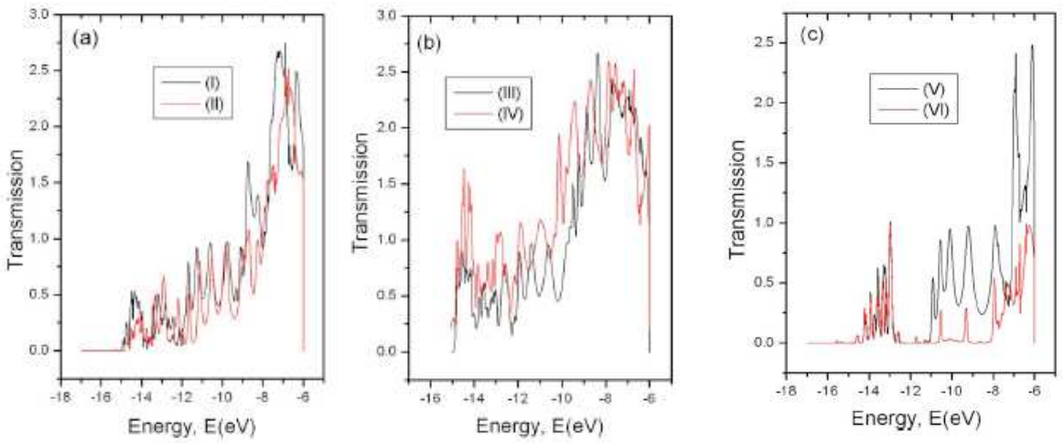

Fig. 14. (Color online) Transmission function *TE* for a series of nanowires and nanochains, with the transmission function of a chain embedded in a carbon tube for comparison: (I) curve for wire 2 (parallel double chains); (II) curve for wire 3 (helical double chains); (III) curve for wire 4 (three helical strands); (IV) curve for wire 5 (four parallel strands); (V) curve for wire 1 (single atomic chain); (VI) curve for the atomic chain embedded in a carbon nanotube.

by metal atoms. They found that the transport property of the single chain was much better than that of the carbon tube surrounded by the metal atoms. The coated shell around the chain would decrease the transmission property of single chain. In our calculations, the carbon tube can be viewed as the coated shell which makes the transmission decrease. To make sure of the coupling between the Ni atomic chain and the electrodes, the studied CNT is shorter than the Ni atomic chain. In our studies, the CNT can be looked upon as an

adsorbate like in Bogozi's study. It is widely accepted that the adsorbate induced conductance change is due to the scattering of the conduction electrons by the adsorbates as the electrons impinge on the surface(Bogozi et al, 2001). The interaction between the CNT and the Ni atomic chain leads to rearrangement of the electrons in system which remarkably influences the transmission of the Ni atomic chain. Nearly the whole surface of the Ni atomic chain is covered by the CNT, which causes a sharp decrease in the transmission.

In Fig. 15, we plot the *I-V* characteristic curves that correspond to the different nanowires. Six *I-V* curves were obtained from different samples, many of which showed the same general, nonlinear, symmetric shape. An interesting point in Fig. 15 is the region around the zero voltage in the I-V curves. For the single atomic chain in Fig. 15(a), a clear flat was observed around the zero voltage, but as for others, the flat was not clear. The slope of the I-V curve for wire 5 is the largest among all the nanowires. Furthermore, the conductance increases with diameter of nanowire. Increasing the diameter of a nanowire therefore appears to improve the transmission area and thus the conductance. A recent experiment (Guo et al, 2003) also showed that a larger diameter yields a larger conductance, as is the case with bulk systems. The experimental results of Ohnishi and Kondo further indicated that the strand number of nanowire would play role in conductance of nanowires. They found that a double strand has twice the unit conductance of a single strand if the interaction between the two individual rows is not strong. Our calculation is consistent with the experimental results of Ohnishi and Kondo.

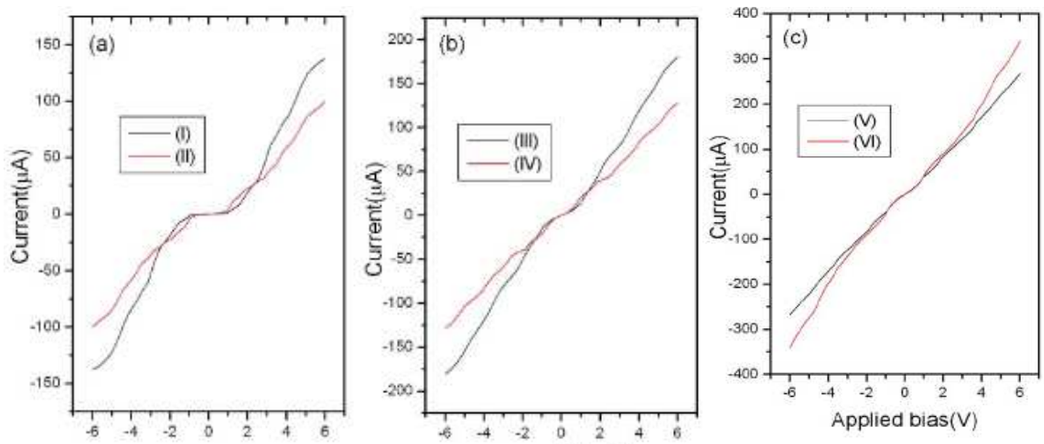

Fig. 15. (Color online) I-V characteristic curves obtained from our calculations: (I) curve for wire 1; (II) curve for wire 2; (III) curve for wire 3; (IV) curve for wire 4; (V) curve for wire 5; (VI) curve for the atomic chain embedded in a carbon nanotube.

It also can be seen in Fig. 15 that the current increases with the external bias. It is clear that the computed *I-V* curve does not follow an ohmic pattern. This is a characteristic feature of nanostructured materials. Due to the observed nonlinear I-V characteristic, there exists no true linear resistivity for all samples. Correia's research results further demonstrated the nonlinear character of *I-V* curves for metallic nanowires(Costa-Kramer et al, 1997), and he suggested that the most plausible explanation for this nonlinear behavior was connected with the Coulomb blockade phenomenon in small conducting systems. We believe that the nonlinear behavior is caused by the quantum size effect. When the size of a metallic nanowire or nanochain is comparable to the electron de Broglie wavelength, electrons in the

nanowire and those transmitted through the nanowire manifest the quantum size effect. Under spatial confinement, the electron energies are also quantized, which leads to many effects. Electron transport in nanowires must be governed by these quantum effects and also by the enhanced boundary scattering. As electrons in a quantum wire are confined, they form quantized standing wave states along the nanowire. This kind of quantum size effect can cause the properties of nanowires and nanochains, such as the oscillation behavior with diameter in *I-V* curves, to differ significantly from those of bulk materials. The difference between the *I-V* curve of the single chain and that of the chain embedded in a carbon nanotube is also clearly noticeable, and the quantum effect between the nanochain and the carbon nanotube causes the nonlinear feature to become quite evident.

4. Melting behavior of 1-D Nickel nanowire

Nanoscale materials have unique properties different from crystal structures. Currently various types of nanodevices are being studied, and, in particular, metallic nanowires receive much attention in both industrial and academic fields because of their magic structure and conductance. Takayanagi's group succeeded in making suspended gold and platinum nanowires(Oshima et al, 2002) in ultrahigh vacuum. Many theoretical studies on ultrathin nanowires have been done using atomistic simulations for several metals, such as Ag (Finbow et al, 1997). Much work has been done for synthesization of nanowire by many new methods(Ono et al, 1997). Genetic algorithm study of the structure of nanowire has been carried out by our research group(Wang et al, 2001). A microscopic description of the melting behavior of nanowire is probably one of the most important problems in physical and material sciences. Simulations have been carried out for nanoscale-width platinum and silver wires. Melting of gold clusters has been investigated to study the thermal evolution of structural and dynamic properties (Cleveland et al, 1999). The thermal properties of ultrathin copper nano-bridges were investigated by Kang (Kang et al, 2002). Although these numerical studies account for the general feature of the melting transition, the microscopic process during the phase transition is still unclear. Experiments have not allowed us to directly observe the melting process. Molecular dynamics (MD) simulations have become a favorite tool for investigating the physics of nanowires theoretically. In this letter, we use MD simulation to address this issue.

4.1 Simulation methodology

We chose to employ the well-fitted tight-binding many body potential with proven ability to reliably model various static and dynamic properties of transition and noble metals. The configurations of nanowires are obtained by the genetic algorithm (GA) previously used by our group with one-dimensional periodical boundary condition along the wire axis direction. The MD time step is chosen as 2.5 fs. The MD simulations start from an initial temperature (400 K). The temperature gradually increases toward final temperature (1500 K) at two heating rates equal to 20 K/ fs and $1x10^{10}$ K/ s, respectively.

4.2 Results and discussion

Figure 16 shows the two kinds growth sequences of nickel nanowires obtained by GA optimization. The nickel nanowire that we studied is multishell structure, which is composed of coaxial cylindrical tubes. Each shell of nickel wire winds up helically by atomic rows. The surface of each shell exhibits a nearly triangular network. W3-1 and W3-2 have

trigonal multishell packing. The thinnest wire W3-1 has a three-strand structure. W5-1 and W5-2 are not helical packing. W5-1 and W5-2 are composed of two-shell and three-shell centered pentagonal structures, respectively.

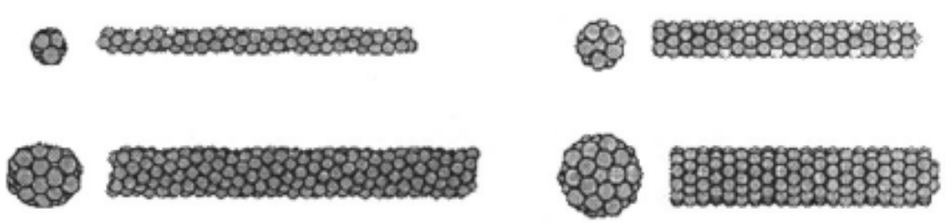

Fig. 16. Morphologies of structural growth sequences in selected nickel nanowires. The nanowire from the top to bottom on the left-hand side corresponds to W3-1, W3-2, and the nanowire from the top to bottom on the right-hand side corresponds to W5-1, W5-2, respectively.

Figure 17 gives us an overall physical picture of the melting process of nanowire. We find that the melting of nanowire starts from the interior atoms. Interestingly, when the slow heating rate is applied, the central atoms first move along the wire axis direction at a rather low temperature, while the helical outer shells are almost invariant. It is worth noting that the moving central atoms are not discrete but to build up a long monostrand atomic chain. The monostrand atomic chain is very stable. The first single atomic chain can exist in a wide temperature region (850–900 K). As the temperature arises, the regular monostrand atomic chain begins to become deformed and finally, the atomic chain is broken to form a new type of cluster.

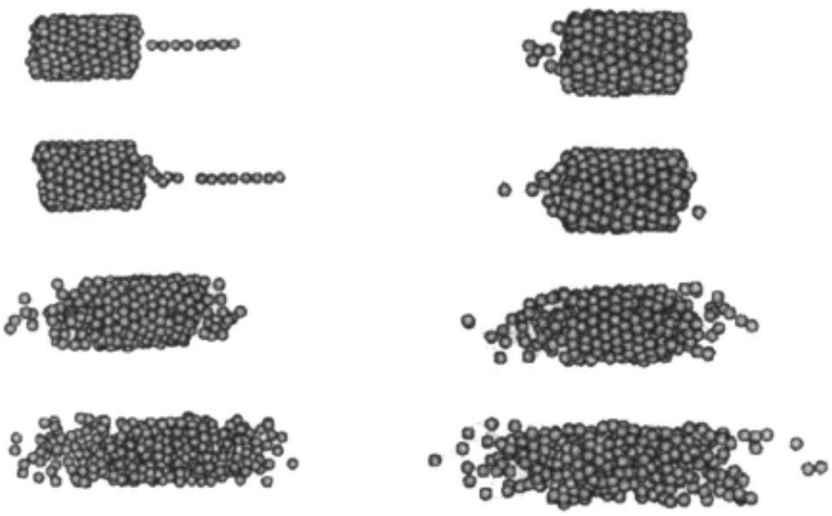

Fig. 17. Structural evolution of nickel nanowire with the temperature increase. The picture from the top to the bottom on the left-hand side corresponds to the 850, 900, 1000, 1050 K, and the picture from the top to the bottom on the right-hand side corresponds to 900, 950, 1050, 1100 K. The pictures on the left-hand side correspond to the heating rate 10^{10} K/s, thepictures on the right correspond to the heating rate 20 K/ s.

The atomic volume(V) and internal energy (E) are the common approaches for monitoring structural changes of the nanowire melting illustrated in Fig. 18. This figure exhibits three temperature regions, denoted by A, B, and C, in which the nanowire behaves differently. At the temperature region A, the atoms are located in well-defined lattice-site equilibrium positions, around which the atoms execute relatively small amplitude motions, with slight variations of interatomic distances, as long as structural changes do not occur. Upon heating the nanowire undergoes a transition from the temperature region A to region B in which atomic volume and internal energy increase very strongly, thus indicating that structural changes occur within the nanowire. With the temperature increase, the system undergoes a transition from region B to region C in which the atomic volume and internal energy is relatively high. It is worth mentioning that, when the slow heating rate is applied in this simulation, the melting temperature becomes low.

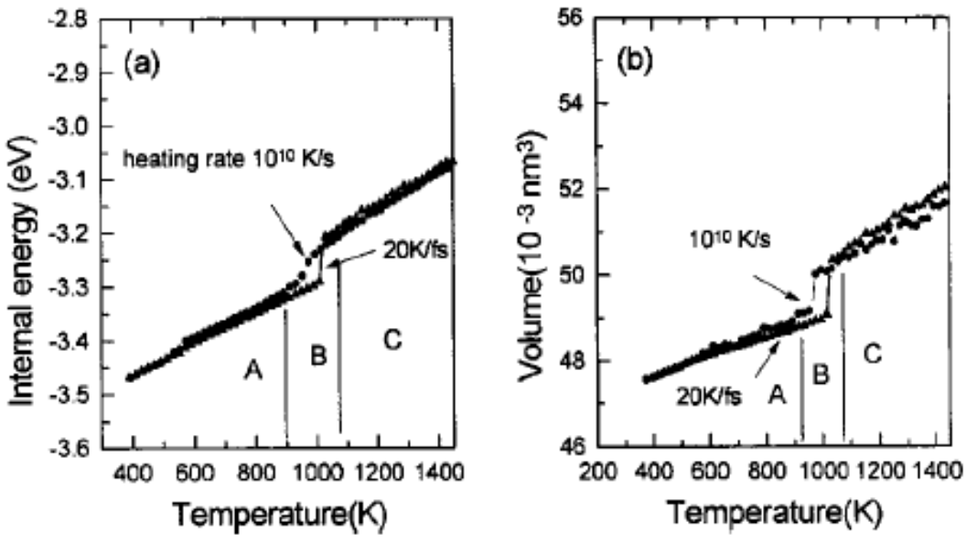

Fig. 18. The internal energy (a) and atomic volume (b) of the nanowire as a function of temperatures.

Figure 19 shows the pair correlation function (PCF) of nanowires at different temperatures. At low temperature, the crystalline structure is highly stable. With increasing temperature the peaks are broadened and lowered. Some peaks are nearly lost. At temperature T=900–1200 K, a diffusion dynamics is thermally activated. This is signaled by the corresponding pair correlation function. Finally, the crystal order is broken and the melting occurs. The shape of the PCF at the temperature 900–1200 K implies that coexistence of liquid and crystal is presented.

To further illustrate the melting phenomena and to distinguish the local symmetry of clusters in the melting process of nanowire, the common bond pair analysis previously used by us is adopted to characterize the local cluster's changes in the melting process of nanowire. In this technique, two atoms are said to be near neighbors if they are within a specified cutoff distance of each other. The first index denotes which peak of the PCF belongs to the pair under consideration; the second one counts the number of common nearest neighbors of that pair; the third one specifies the number of particles denoted by the second one; a fourth one sometimes is necessary to distinguish configurations having the

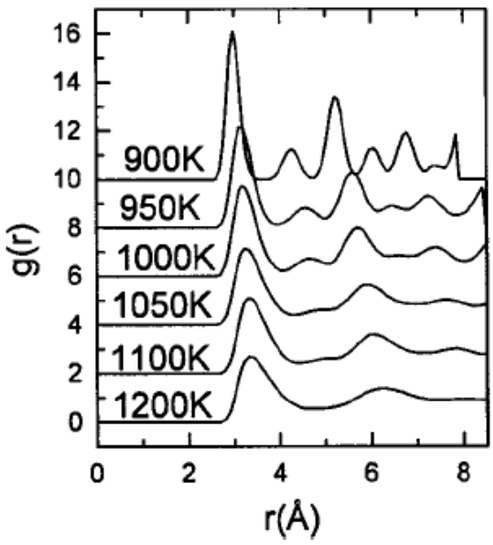

Fig. 19. The pair correlation functions at different temperatures in the melting process of nanowire.

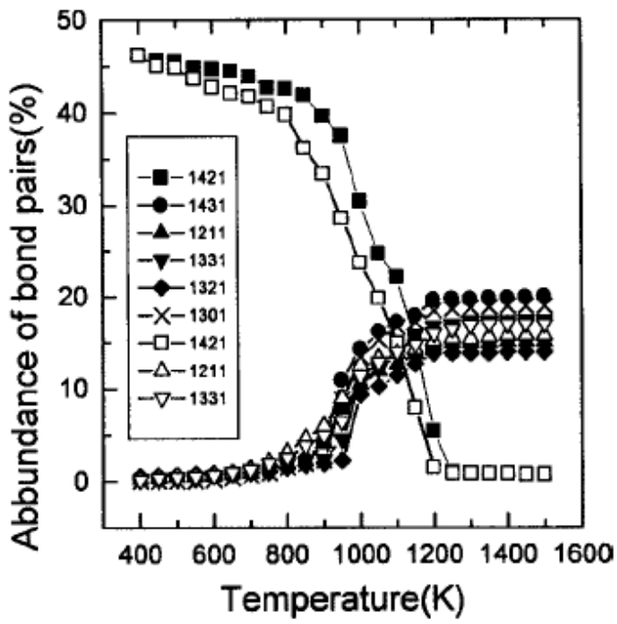

Fig. 20. Abundance of selected local clusters as a function of temperatures. Open symbol corresponds to the heating rate 10^{10} K/ s, solid symbol corresponds to the heating rate 20 K/ fs.

first three indices equal, yet topologically different. This method is able to distinguish various local structures between fcc, hcp, bcc, and the icosahedral structures. The fcc structure has the type 1421 bond pair, whereas the hcp crystal has the equal number of 1421 and 1422 bond pairs. The 1201 and 1311 bond pairs represent the rhombus symmetrical features of short-range order. Fig. 20 shows the evolution of the local cluster during the

melting process of the nanowire. The increase in the abundance of the local clusters 1331, 1321, 1311, etc., and the decrease of the clusters 1421 indicate the occurrence of the melting of nanowire. The fcc structure in nanowire is presented through the existence of 1421 pairs, but not found in liquid from the melting of nanowire. The pairs 1421 are the main components in the nanowire. The overall melting point of nanowire can be defined as 1050 K from the sudden changes of local cluster curves. The local clusters in liquid from the nanowire melting are not decahedron, but rhombus symmetrical structures.

Our simulation result shows that as a result of melting process the amount of rhombus symmetric structure reduces in favor of the crystalline order. During the melting process, the local cluster 1421 in nanowire would decompose into other local clusters such as 1311 and 1321, etc. Local cluster diffusion leads to the occurrence of the melting. Cluster diffusion from equilibrium position is the main melting features of nanowire. Because there is frustration which comes from the difficulty in close packing with perfect cluster in flat three-dimensional space, therefore liquid cannot be composed of only one kind of cluster. The existence of various local clusters in liquid just meets the packing demand. Therefore a suitable proportion of local cluster is an important character for the nanowire melting. With the temperature increase, the local cluster begins to diffuse; this will lead to some new defects in nanowires. These defects would cause the decease of the average binding energy. The nanowires with a lot of defects should have lower thermal stability. Therefore, defect would accelerate the melting of the nanowire. Figure 20 shows that the evolution of the local cluster at two different heating rates is quite different. The transition temperature at slow heating rate is lower than that at fast heating rate.

It must be pointed that the 1421 represents the fcc microcrystal structural unit rather than integrals. 1431, 1331, 1321, 1301, and 1211 are also clusters which are ordered structures. Nickel nanowire contains a lot of 1421 microcrystal units. In this study, as the temperature increases, not only is diffusion of single atom observed, but also the diffusion of local clusters is found. Therefore, we think the nanowire melting is due to the diffusion of local clusters. In Fig. 20, the clusters 1421, 1431, 1331, 1321, etc., are, in fact, some leftover crystal units. The existence of these leftover crystal structural units implies that there are some leftover crystal units in liquid resulting from the nanowire melting. That is to say, the fact that some small crystal structural units moves from the nanowire causes the beginning of the nanowire melting. Melting behaviors of other nanowires with different diameters are also studied. It is noted that the melting point depends on the diameter size. In general, larger diameter would cause higher melting point. To explore the size dependence of nanowire melting temperature, we plot the overall melting temperature Tm versus wire diameter (D) in Fig. 21.

The T_m for the wires with the hexagonal growth sequence fit well to a linear dependence as $T_m = T_0 - \delta/D$, where T_0=1638K is the extrapolated melting temperature at the infinite limit, δ=857 K nm describes the linear dependence of T_m with wire diameter D (in units of nanometers). (When the slow heating rate is applied, T_0=1503 K, δ=782.57 K nm.) Such 1/D dependence of melting temperature for nanowire is similar to the well-known size relationship for metal nanoclusters. The heating rate has great influence on the melting temperatures of nanowires. The melting point at the slow heating rate is lower than that at the fast melting point. As compared with the linear size dependence for the hexagonal wires, almost belong to the same size relationship while the T_m of other nanowires deviate from such linear fit. These differences indicate that the atomic structures of nanowires play a significant role in determining the melting behavior of nanowires.

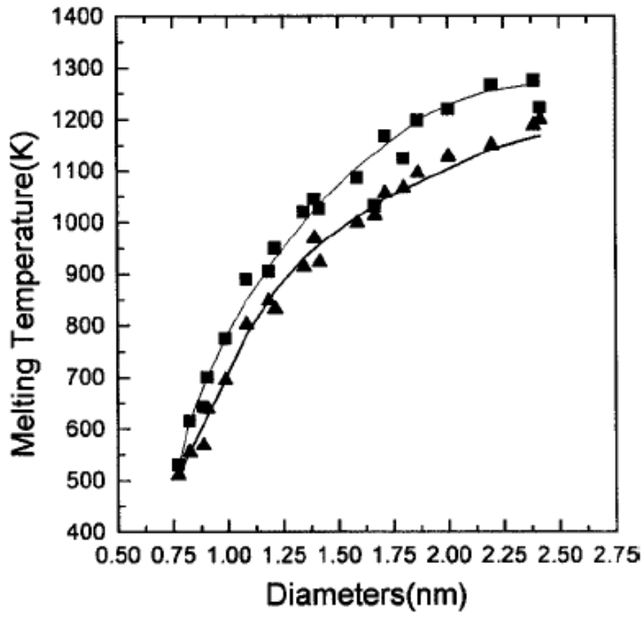

Fig. 21. Overall melting temperature T_m *(K)* vs nanowire diameters D (nm). The square symbol and the top line correspond to the heating rate 20 K/ fs, and the triangular symbol and the bottom line correspond to the heating rate $1x10^{10}$K/s, respectively.

5. Conclusion

Our simulation results have shown three aspects of properties of nanowires which are as follows:

1. Simulation results indicate that the maximum tensile strain of carbon nanowire is up to 245% before tensile failure. The maximum stress for a CNW is 16.65 GPa which is lower than that of the carbon nanotubes. During the elongation process, a stable single atomic chain is obtained just like to draw a silk from a cocoon. The superplastic properties of carbon nanowires could prove useful in the fabrication of carbon nanocomposites.
2. This composite of CNW@CNT undergoes a large elongation in which a pentagon–heptagon dislocation (5|7) defect, octagonal defects and higher-order rings are observed. Insertion of the CNW into CNT increases the plastic elongation of a CNW@CNT under axial stretching. As the strain continues to increase, the composite structure is found to become a long single carbon atomic chain. Interestingly, insertion of the CNW into CNT does not increase the critical strength of the CNT but weaken. A large hole caused by (5|7) defect make the carbon tube fracture easily.
3. The electronic transport properties of these nanostructures have been studied, and we find that transmission is dependent on the geometric structures of nanowires and their size of diameters. Because of the quantum size effect, the I-V curves of the nanowires are clearly nonlinear, which does not follow an ohmic pattern.
4. Molecular dynamics simulation has been performed to study the melting process of nanowire by means of a tight binding model potential. We set up in the present work a general picture of the physical process which governs the melting phenomenon in nickel nanowire. The atomic volume, internal energy, the pair correlation function, and

the local clusters provide a strong and clear signature of structural changes as the melting occurs in nanowire. The thermal stability of nickel nanowires is dependent on the structures and size of the nanowire; the melting temperature of nickel nanowire is lower than the bulk's.

6. Acknowledgements

We would like to acknowledge the support from the National Natural Science Foundation of China [Grant Nos.50971081, 50831003, 50871062 and 50772061] and the National Basic Research Program of China [Grant No.2007CB613901]. This work is supported by a grant from the National Science Fund for Distinguished Young Scholars [Grant No. 50625101] and Scientific Research Foundation for Returned Scholars [Grant No. JIAO WAI SI LIU2007–1108], Ministry of Education of China. We also thank the support from the Natural Science Fund for Distinguished Young Scholars of Shandong [Grant No. JQ200817]. This work is also supported by the Natural Science Fund of Shandong Province (ZR2009FM043). This work was supported by the Ph. D. programs foundation of ministry of education of China (No. 20090131110025).

7. References

Li, H.; Sun, F.W.; Li, Y.F.; Liu, X.F. & Liew, K.M. (2008). Theoretical studies of the stretching behaviour of carbon nanowires and their superplasticity, Scripta Mater, Vol. 59, 479-482.

Li, H.; Sun, F.W.; Liew, K.M. & Liu, X.F. (2009) Stretching behavior of a carbon nanowire encapsulated in a carbon nanotube, Scripta Mater, Vol. 60, 129-132.

Li, H.; Zhang, X. Q.; Sun, F. W.; Li, Y. F.; Liew, K. M.; He, X. Q. (2007). Theoretical study of the electrical transport of nickel nanowires and a single atomic chain, J. Appl. Phys, Vol. 102, 013702.

Li, H.; Pederiva, F. & Wang G. H. (2005). How does the Nickel Nanowire Melt? Appl.Phys.Letts, Vol. 86(1), 011913.

Ribarsky, M.W. & Landman, U. (1988). Dynamical simulations of stress, strain, and finite deformations, Phys. Rev. B, Vol. 38, 9522-9537.

Brenner, D.W.; Shenderova, O.A.; Harrison, J.A.; Stuart, S.J.; Ni, B. & Sinnott, S.B. (2002). A second-generation reactive empirical bond order (REBO) potential energy expression for hydrocarbons, J. Phys.: Condens. Mater, Vol. 14, 783-802.

Sinnott, S.B.; Shenderova, O.A.; White, C.T. & Brenner, D.W. (1988). Mechanical Properties of Nanotubule Fibers and Composites Determined from Theoretical Calculations and Simulations, Carbon, Vol. 36, 1-9.

Shenderova, O.A. & Brenner, D.W. (2000). Atomistic modeling of the fracture of polycrystalline diamond, Phys. Rev. B, Vol. 61, 3877-3888.

Huhtala, M.; Krasheninnikov, A.V.; Aittoniemi, J.; Stuart, S. J.; Nordlund, K. & Kaski, K. (2004). Improved mechanical load transfer between shells of multiwalled carbon nanotubes, Phys. Rev. B, Vol. 70, 045404.

Stuart, S.J.; Tutein, A.B. & J.A. Harrison. (2000). A reactive potential for hydrocarbons with intermolecular interactions, J. Chem. Phys, Vol. 112, 6472.

Sammalkorpi, M.; Krasheninnikov, A.; Kuronen, A.; Nordlund, K. & Kaski, K. (2004). Mechanical properties of carbon nanotubes with vacancies and related defects, Phys. Rev. B, Vol. 70, 245416.

Belytschko, T.; Xiao, S. P.; Schatz, G.C.& R.S. Ruoff, (2002). Atomistic simulations of nanotube fracture, Phys. Rev. B, Vol. 65, 235430

Gear, C.W. (1971). Numerical Initial Value Problems in Ordinary Differential Equations, Prentice-Hall, New Jersey, USA.

Liew, K.M.; Wong, C.H.; He, X.Q.; Tan, M.J. & S.A. Meguid, (2004). Nanomechanics of single and multiwalled carbon nanotubes, Phys. Rev. B, Vol. 69, 115429.

Wang, Q.; Duan, W.H.; Liew, K.M. & X.Q. He, (2007). Local buckling of carbon nanotubes under bending, Appl. Phys.Lett. Vol. 90, 033110.

Nose, S. (1984). A molecular dynamics method for simulations in the canonical ensemble, Mol. Phys. Vol. 52, 255–268.

Hoover, W.G. (1985). Canonical dynamics: Equilibrium phase-space distributions, Phys. Rev. A, Vol. 31, 1695-1697.

Asaka, K.; Kizuka, T. (2005). Atomistic dynamics of deformation, fracture, and joining of individual single-walled carbon nanotubes, Phys. Rev. B, Vol. 72, 115431.

Ogata, S.; Shbutani, Y. (2003). Ideal tensile strength and band gap of single-walled carbon nanotubes, Phys. Rev. B, Vol. 68, 165409.

Liew, K.M.; He, X.Q. & C.H. Wong, (2004), On the study of elastic and plastic properties of multi-walled carbon nanotubes under axial tension using molecular dynamics simulation, Acta Mater. Vol. 52, 2521.

Yu, M. F.; Files, B.S. & R.S. Ruoff, (2000). Tensile loading of ropes of single wall carbon nanotubes and their mechanical properties, Phys. Rev. Lett. Vol. 84, 5552.

Lennard-Jones, L.E. (1924). On the Determination of Molecular Fields. I. From the Variation of the Viscosity of a Gas with Temperature, Proc. R. Soc. Lond. Ser. A ,Vol. 106, 441.

Troiani, H. E.; Miki-Yoshida, M.; Camacho-Bragado, G. A.; Marques, M. A.; Rubio, L. A.; Ascencio, J. A. & Jose-Yacaman, M. (2003). Direct Observation of the Mechanical Properties of Single-Walled Carbon Nanotubes and Their Junctions at the Atomic Level, Nano Lett. Vol. 3, 751-755.

Nardelli, M. B.; Yakobson, B. & Bernholc, J. (1998). Mechanism of strain release in carbon nanotubes, Phys.Rev. B, Vol. 57, R4277-R4280.

Lehtinen, P. O.; Foster, A. S.; Ayuela, A.; Krasheninnikov, A.; Nordlund, K. & Nieminen, R. M. (2003). Magnetic Properties and Diffusion of Adatoms on a Graphene Sheet, Phys. Rev. Lett. Vol. 91, 017202.

Strano, M.S. et al., (2003). Electronic Structure Control of Single-Walled Carbon Nanotube Functionalization, Science. Vol. 301, 1519-1522.

Rinzler, A. G.; Hafner, J. H. & Nikolaev, P. (1995). Unraveling nanotubes: field emission from an atomic wire, Science. Vol. 269, 1550-1553.

Wang, Y.; Ning, X. J.; Lin, Z. Z.; Li, P. & Zhuang, J. (2007). Preparation of long monatomic carbon chains: Molecular dynamics studies, Phys. Rev. B, Vol.76, 165423.

Demczyk, B. G.; Wang, Y. M.; Cumings, J.; Hetman, M.; Han, W.; Zettl, A. & R. O. Ritchie, (2002). Direct mechanical measurement of the tensile strength and elastic modulus of multiwalled carbon nanotubes, Mater. Sci. Eng. A, Vol. 334, 173-178.

Troiani, H.E.; Miki-Yoshida, M.; Camacho-Bragado, G. A.; Marques, M. A. L.; Jose-Yacaman, M. & Rubio, A. (2004). Direct Observation of the Mechanical Properties of Single-Walled Carbon Nanotubes and Their Junctions at the Atomic Level, Nano Lett. 4 811-815.

Lu, L.; Li, S.X. & Lu, K. (2001). An abnormal strain rate effect on tensile behavior in nanocrystalline copper, Scripta Mater. Vol. 45 1163-1169.

Krans, J. M.; Ruitenbeek, J. M. V; Fisun, V. V.; Yanson, J. K. & deJongh, L. J. (1995). The signature of conductance quantization in metallic point contacts, Nature, Vol. 375, 767-769.

Sen, P.; Ciraci, S.; Buldum, A. & I. P. Batra, (2001). Structure of aluminum atomic chains, Phys. Rev. B, Vol. 64, 195420.

Gambardella, P.; Blanc, M.; Brune, H.; Kuhnke, K. & K. Kern, (2000). One-dimensional metal chains on Pt vicinal surfaces, Phys. Rev. B, Vol. 61, 2254.

Kondo, Y.; Takayanagi, K. (2000). Synthesis and Characterization of Helical Multi-Shell Gold Nanowires , Science, Vol. 289, 606-608.

Rodrigues, V.; Fuhrer, T.; Ugarte1, D. (2000). Signature of Atomic Structure in the Quantum Conductance of Gold Nanowires, Phys. Rev. Lett, Vol. 85 (19), 4124-4127.

Garcia-Mochales, P.; Serena, P. A. (1997). Disorder as Origin of Residual Resistance in Nanowires, Phys. Rev. Lett, Vol. 79, 2316-2319.

Burki, J.; Stafford, C. A.; Zotos, X. & Baeriswyl, D. (1999). Cohesion and conductance of disordered metallic point contacts, Phys. Rev. B, Vol. 60, 5000-5008.

Brandbyge, M.; Yacobsen, K. W.; Norskov, J. K. (1997). Scattering and conductance quantization in three-dimensional metal nanocontacts, Phys. Rev. B, 55, 2637-2650.

Enomoto, A.; Kurokawa, S. & Sakai, A. (2002). Quantized conductance in Au-Pd and Au-Ag alloy nanocontacts, Phys. Rev. B, Vol. 65,125410.

Perdew, J. P.; Burke, K.; Ernzerhof, M. (1996). Generalized Gradient Approximation Made Simple, Phys. Rev. Lett, Vol. 77, 3865-3868.

Damle, P. S.; Ghosh, A. W. & Datta, S. (2002). First-principles analysis of molecular conduction using quantum chemistry software, Chem. Phys, Vol. 281,171-187.

Ke, S. H.; Yang, W. & H. U. Baranger, (2006). Nanotube-metal junctions: 2- and 3-terminal electrical transport, J. Chem. Phys, Vol. 124, 181102.

Bogozi, A.; Lam, O.; He, H.; Li, C.; Tao, N. J. L.; Nagahara, A.; Amlani, I. & Tsui, R. (2001). Molecular Adsorption onto Metallic Quantum Wires, J. Am. Chem. Soc, Vol. 123, 4585-4590.

Guo, A. J.; Wang, Q.; Lundstrom, M. & Dai, H. (2003). Ballistic Carbon Nanotube Transistors, Nature, Vol. 424, 654-657.

Costa-Kramer, J. L.; Garcia, N.; Garcia-Mochales, P.; Serena, P. A.; Marques, M. I. & Correia, A. (1997). Conductance quantization in nanowires formed between micro and macroscopic metallic electrodes, Phys. Rev. B, Vol. 55, 5416-5424.

Oshima, Y.; Koizumi, H.; Mouri, K.; Jirayama, H.; & Takayanagi, K. (2002). Evidence of a single-wall platinum nanotube, Phys.Rev. B, Vol. 65, 121401.

G. M. Finbow, R. M. Lynden-Bell, and I. R. McDonald, (1997). Atomistic simulation of the stretching of nanoscale wires, Mol. Phys, Vol. 92, 705-714.

Ono, T. Saitoh, H. & Esashi, M. (1997). Si nanowire growth with ultrahigh vacuum scanning tunneling microscopy, Appl. Phys. Lett, Vol. 70, 1852.

Wang, B. L.; Yin, S. Y.; Wang, G. H. & Zhao, J. J. Novel structures and properties of gold nanowires, (2001). Phys. Rev. Lett, Vol. 86, 2406

Cleveland, C. L.; Luedtke, W. D. & Landman, U. (1999). Melting of gold clusters, Phys. Rev. B, Vol. 60, 5065-5077.

Kang J. W. & Hwang, H. J. (2002). Thermal properties of ultra-thin copper nanobridges, Nanotechnology, Vol. 13, 503-509.

Nanowires Science and Technology

Edited by Nicoleta Lupu

ISBN 978-953-7619-89-3
Hard cover, 402 pages
Publisher InTech
Published online 01, February, 2010
Published in print edition February, 2010

This book describes nanowires fabrication and their potential applications, both as standing alone or complementing carbon nanotubes and polymers. Understanding the design and working principles of nanowires described here, requires a multidisciplinary background of physics, chemistry, materials science, electrical and optoelectronics engineering, bioengineering, etc. This book is organized in eighteen chapters. In the first chapters, some considerations concerning the preparation of metallic and semiconductor nanowires are presented. Then, combinations of nanowires and carbon nanotubes are described and their properties connected with possible applications. After that, some polymer nanowires single or complementing metallic nanowires are reported. A new family of nanowires, the photoferroelectric ones, is presented in connection with their possible applications in non-volatile memory devices. Finally, some applications of nanowires in Magnetic Resonance Imaging, photoluminescence, light sensing and field-effect transistors are described. The book offers new insights, solutions and ideas for the design of efficient nanowires and applications. While not pretending to be comprehensive, its wide coverage might be appropriate not only for researchers but also for experienced technical professionals.

INTECH
open science | open minds

InTech Europe
University Campus STeP Ri
Slavka Krautzeka 83/A
51000 Rijeka, Croatia
Phone: +385 (51) 770 447
Fax: +385 (51) 686 166
www.intechopen.com

InTech China
Unit 405, Office Block, Hotel Equatorial Shanghai
No.65, Yan An Road (West), Shanghai, 200040, China
中国上海市延安西路65号上海国际贵都大饭店办公楼405单元
Phone: +86-21-62489820
Fax: +86-21-62489821

IntechOpen